JOURNAL OF AIRCRAFT
Vol. 41, No. 4, July–August 2004

Analysis, Design, and Optimization of Noncylindrical Fuselage for Blended-Wing-Body Vehicle

V. Mukhopadhyay* and J. Sobieszczanski-Sobieski†
NASA Langley Research Center, Hampton, Virginia 23681
and
I. Kosaka,‡ G. Quinn,§ and G. N. Vanderplaats¶
Vanderplaats R&D, Inc., Colorado Springs, Colorado 80906

A study toward finding an efficient noncylindrical fuselage configuration for a conceptual blended-wing-body flight vehicle is presented. A simplified two-dimensional beam-column analysis and optimization was used to demonstrate the problem of containing cabin pressure in such flight vehicles. Then a set of detailed finite element models of deep sandwich panel and ribbed shell construction concepts were analyzed and optimized. Generally these constructions with high bending stiffness but without curvature were found to be structurally efficient to a certain extent to withstand internal pressure and resultant compressive loads simultaneously. To attain additional structural efficiency, a set of multibubble fuselage configurations was developed for balancing internal cabin pressure load efficiently, through membrane stress in inner-stiffened shell and intercabin walls. An outer-ribbed shell was designed to prevent buckling due to external resultant compressive loads. Initial results from finite element analysis of a representative fuselage segment, using this stress separation concept, appear to be promising. This concept has some additional advantages. Distortion of aerodynamic surface due to cabin pressure is minimal. Availability of duct space above and below the main fuselage can be used for direct ventilation; these also provide structural redundancy in the event of a pressure leak as well as for improved crashworthiness. These concepts should be developed further to exploit their inherent structural efficiency.

I. Introduction

IN the revolutionary blended-wing-body (BWB) megatransport concept,[1,2] the pressurized lifting-body fuselage must be designed to resist internal cabin pressure and buckling due to high overall bending load. These loads combine in a nonlinear manner to induce severe deformation and high stresses that might necessitate significant structural weight penalty. In addition, resulting deformation of the aerodynamic surface could significantly affect performance advantages provided by the lifting body. Similar design problem also exist for conformal shaped propellant tanks of reusable launch vehicles.[3] This problem was investigated for Airbus-type elliptic-section composite fuselage[4] as well as for BWB[1,5] and X33[3] with special sandwich composite skin and metal honeycomb core. In previous BWB studies,[6,**] effects of cabin shape and volume were investigated from a baseline configuration using an aerodynamic-based optimization scheme, but structural design with internal pressure or buckling issues were not addressed. In another BWB conceptual structural design study,[5] several promising noncylindrical fuselage configurations were identified but no optimization was done.

Following the lessons learned in Ref. 5, this paper presents new sizing, analysis, design, and optimization results toward finding an efficient noncylindrical BWB configuration, considering both internal pressure and compressive load including buckling stability. A simplified two-dimensional beam-column analysis and optimization was first used to demonstrate the problem of containing cabin pressure in such flight vehicles. Then a set of detailed finite element models of deep sandwich panel and ribbed shell construction concepts were analyzed and optimized with stress and buckling constraints. The four idealized deep sandwich and ribbed shell configurations that represent a critical upper surface panel section are shown in Fig. 1.

To attain additional structural efficiency, several multibubble stiffened fuselage section concepts were developed. This special configuration resists internal pressure load through membrane stress balance while resisting bending and compression load with an outer stiffened ribbed shell. The multibubble concept was then refined further to meet critical design requirements with minimal weight increment.

The knowledge gained in this conceptual design study would provide the designers with options to make the BWB revolutionary concept both structurally feasible and aerodynamically efficient. This could also give BWB development a competitive advantage over the Airbus[7] A380 in the lucrative 500–800 passenger long-range travel markets.

II. Two-Dimensional Beam-Column Analysis

Some initial sizing, stress, and deflections were estimated using analytical nonlinear beam-column solutions[8] for a two-dimensional simply supported beam representing a simplified cabin roof that acts as a surface of a pressure vessel and as a compressed flange of a beam in bending. Maximum deflection $z_{\max}$, bending moment $M_{\max}$, and stress $\sigma_{\max}$ at midspan for simply supported boundary conditions are given by Eqs. (1–3):

$$z_{\max} = \frac{5pr \cdot l^4}{384EI} \frac{12(2\sec\mu - 2 - \mu^2)}{5\mu^4} \tag{1}$$

Presented as Paper 2002-5664 at the AIAA/ISSMO 9th Symposium on Multidisciplinary Analysis and Optimization, Atlanta, GA, 4–6 September 2002; received 3 January 2003; revision received 3 July 2003; accepted for publication 7 July 2003.

*Senior Research Engineer, Systems Analysis Branch; v.mukhopadhyay-1@nasa.gov. Associate Fellow AIAA.
†Senior Research Scientist, Analytical and Computational Methods Branch; j.sobieski@larc.nasa.gov. Fellow AIAA.
‡Senior Researcher; ikosaka@vrand.com.
§Senior Researcher; quinng@vrand.com.
¶President; vanderplaats@vrand.com. Fellow AIAA.

**Smith, H., et al., "Blended Wing Body Airliner: Air Vehicle Design," Cranfield University Design Report Data available online at http://www.wing.cranfield.ac.uk/[cited 1999].

Table 1 Summary of results: Two-dimensional beam column and three-dimensional panel FEM analysis and optimization

	Initial				Optimized					
Concept	Depth, m	Skin t, m	P/P_{cr}	Wt/area, kg/m^2	Depth, m	Skin, m	P/P_{cr}	Max disp., m	Material	Wt/area, kg/m^2
2D HC Beam	0.150	0.006	0.40	42.44	0.2642	0.0045	0.18	0.0300	AL	37.9
Flat HC	0.137	0.003	0.50	15.3	0.2007	0.0046	0.66	0.0086	comp	24.1
Flat ribbed	0.152	0.003	0.50	13.5	0.1842	0.0058	0.66	0.0064	comp	25.6
Flat HC + Cat	0.167	0.003	0.50	15.4	0.0201	0.0046	0.71	0.0090	comp	24.2
Vaulted HC	0.200	0.003	——	17.01	0.1702	0.0033	0.66	0.0112	comp	25.4

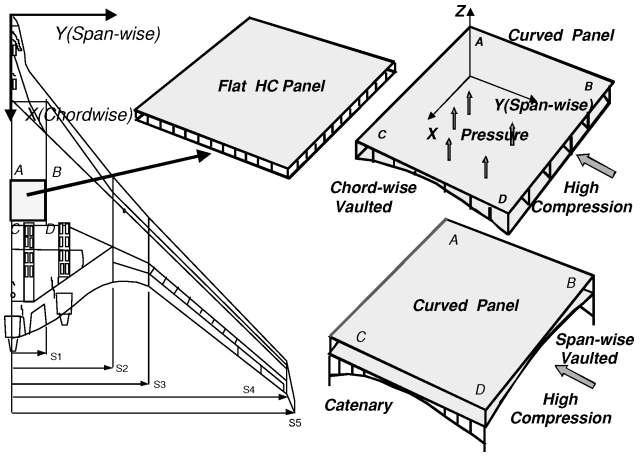

Fig. 1 Conceptual configurations of flat and curved top surface panel.

$$M_{\max} = \frac{pr \cdot l^2}{8} + \frac{5pr \cdot l^4}{384EI}\frac{12(2\sec\mu - 2 - \mu^2)}{5\mu^4}P \qquad (2)$$

$$\sigma_{\max} = M_{\max}\frac{\mathrm{d}}{2I} + \frac{p}{2Wt} \qquad (3)$$

where

$$P_{cr} = \pi^2 EI/l^2 \qquad \text{and} \qquad \mu = (\pi/2)\sqrt{P/P_{cr}}$$

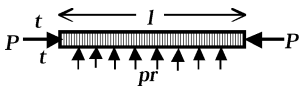

and where P is distributed axial compressive load, pr is transverse cabin pressure load, I denotes bending moment of inertia, E is Young's modulus, and l is column length as shown in the sketch. Note that stresses and deflections from Eqs. (1) and (2) diverge as P approaches critical compressive buckling load P_{cr}. Let us assume $I = 0.5tw(d-t)^2$, where d is beam depth, t is the thickness of the top and bottom flange or face sheet, and w is unit width. Initially let us assume face skin thickness $t = 0.006$ m, beam depth $d = 0.15$ m, beam length $l = 3.5$ m, transverse pressure $pr = 84{,}830$ Pa (12.3 pounds per square inch), and axial compressive load $P = 165{,}000$ kg/m. The face sheet material of the sandwich was assumed to be aluminum AL7075-T6 with Young's modulus $E = 7.1 \times 10^{10}$ Pa, allowable stresses $F_{tu} = 5.24E{+}8$ Pa, $F_{ty} = 4.55E{+}8$ Pa, and $F_{cy} = 4.62E{+}8$ Pa.

The resulting buckling load ratio P/P_{cr} was close to 0.4. The nondimensional midspan deflection ratio $Z_{\max}/d$ is shown in Fig. 2. The maximum compressive stress ratio $\sigma_{\max}$/yield stress F_{cy} is shown in Fig. 3 and the maximum bending moment ratio $M_{\max}/(prl^2/8)$ variations with P/P_{cr} are shown in Fig. 4. Figure 2 indicates that, for $P/P_{cr} = 0.4$, midspan deflection is about 40% of beam depth. Figure 3 shows that the maximum combined compressive stress $\sigma_{\max}$ is about 80% of the allowable compressive yield stress F_{cy}. Figure 4 shows that for this beam column, additional bending moment caused by beam deflection is almost 40% of that due to transverse pressure load alone. The top and bottom flange or skin panel weighs about 36 kg/m^2, and the honeycomb core weighs 6.4 kg/m^2. A quick spreadsheet-based weight optimization was performed with beam depth and skin thickness as design

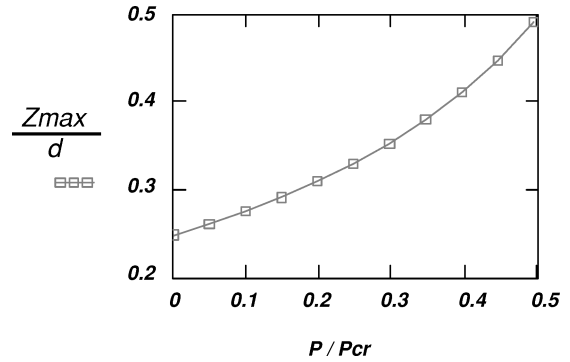

Fig. 2 Midspan deflection $Z_{\max}$/beam depth vs compressive load P/P_{cr} for an idealized simply supported beam column [Aluminum AL-7079: $d = 0.15$ m, $t = 0.006$ m, $l = 3.5$ m, $P = 165{,}000$ kg/m, $pr = 84{,}830$ Pa (12.3 psi)].

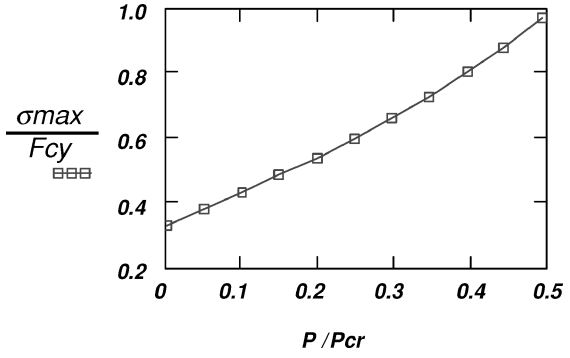

Fig. 3 Maximum compressive stress ratio $\sigma_{\max}/F_{cy}$ vs compressive load P/P_{cr}.

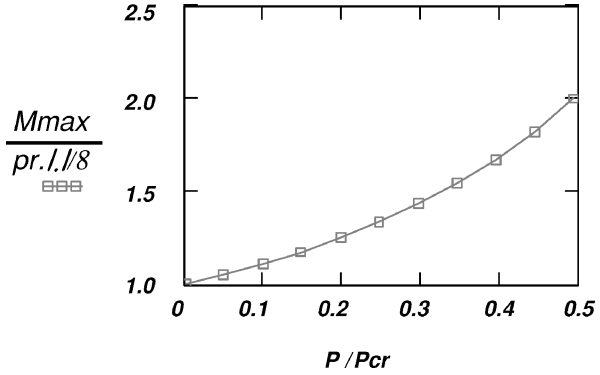

Fig. 4 Maximum bending moment ratio $M_{\max}/(pr \cdot l^2/8)$ vs compressive load P/P_{cr}.

variables and $P/P_{cr} < 0.66$, $Z_{\max}/d < 1$, and $\sigma_{\max}/F_{cy} < 1$ as constraints. Results are presented in Table 1. The unit weight ratio was reduced to 38 kg/m^2 by increasing d to 0.026 m and reducing t to 0.0045 m.

This simple but conservative nonlinear analysis and optimization was used for sizing the three-dimensional concepts. This also illustrates the weight penalty and high-stress problem associated with resisting normal pressure by bending stress. In this beam of length l,

bending stress is proportional to $(pr \cdot l^2)/(d \cdot t)$, whereas in a cylindrical pressure vessel of radius R, the resulting membrane stress is proportional to $(pr \cdot R/t)$. Assuming R is of same order as l, the beam has much higher stress and is consequently much heavier. The problem is aggravated by the nonlinear effect of compressive load acting on the deflected beam or plate. So to obtain an efficient structure, one must increase the bending stiffness using a deep sandwich shell with lightweight high-strength composite skin and honeycomb core. This investigation is described next.

III. Panel Finite Element Method Analysis

Four idealized top fuselage surface composite panel configurations were analyzed and optimized for minimum weight under internal pressure and estimated compressive loads with both stress and buckling constraints. These finite element analyses and optimization were done using a tool described in Ref. 9.

Figure 1 shows the possible location of this critical top surface panel on a BWB planform. These four panel configurations, namely, 1) flat honeycomb sandwich panel, 2) flat double-skin cross-ribbed panel, 3) flat honeycomb panel with spanwise catenary, and 4) spanwise vaulted shell with rod stiffeners are shown in Figs. 5–8, respectively. Estimates of design loads at $2.5g$ flight condition were obtained from previous BWB analyses.[1,2] In addition to an internal cabin pressure load of 84,830 Pa, these panels were subjected to an estimated resultant spanwise compressive load of 165,000 Kg/m and a chordwise tensile load of 12,500 Kg/m. An orthotropic graphite–epoxy composite material was used for the skin and aluminum honeycomb was used for the sandwich core.[1,2,5] Two sets of approximate boundary conditions were used, as shown in Figs. 5 and 8, respectively. Rigid elements were used at some edges for compatibility. Edge elements at the boundary were excluded for stress-constraint evaluation to prevent local stresses from applied boundary conditions from driving the design.

A. Flat Honeycomb Sandwich Panel

A baseline graphite–epoxy composite sandwich 3.5×3.8 m^2 rectangular panel with 0.003-m thick top and bottom skin and a honeycomb core was first considered. The panel depth and skin thickness were treated as design variables. The baseline panel weight was about 15.3 kg/m^2. The constrained optimized weight with the first set of boundary conditions increased to 28.5 kg/m^2. With the second set of boundary conditions, optimized weight was close to 24.5 kg/m^2. A summary of result is presented in Table 1.

B. Flat Double-Skin Ribbed Panel

A baseline double-skin cross-ribbed panel of the same dimension was also analyzed as an alternative to thick honeycomb panel. The panel depth, web, and skin thickness were treated as design variables. The baseline graphite–epoxy ribbed panel weight was about 13.5 kg/m^2 with 14 chordwise ribs and 16 spanwise ribs at 0.25-m intervals. Based on simple plate buckling analysis,[10–12] spanwise and chordwise cross-rib spacing was determined to prevent local panel buckling. Figure 9 shows initial results of this double-skin ribbed panel optimization with only internal pressure load and stress constraints. The optimizer tended to increase the lower skin thickness and panel depth, while reducing the spanwise and chordwise rib thickness. This resulted in marginal weight reduction by about 18%.

However, with both stress and buckling constraints, under the estimated compressive load, the skin thickness increased significantly after optimization. Consequently, the weight (objective function) of the optimized panel with the first set of boundary conditions actually increases by over 240% as shown in Fig. 10. With the second set of boundary conditions, and edge elements excluded, the results were somewhat reasonable. Optimized panel weight was 25.6 kg/m^2. The fine-mesh finite element method (FEM) model exhibited several local buckling modes, due to the manner in which the compressive loads were applied at nodes, and represented the bending loads approximately. Hence, a coarse mesh was used to capture overall panel buckling modes for optimization purposes.

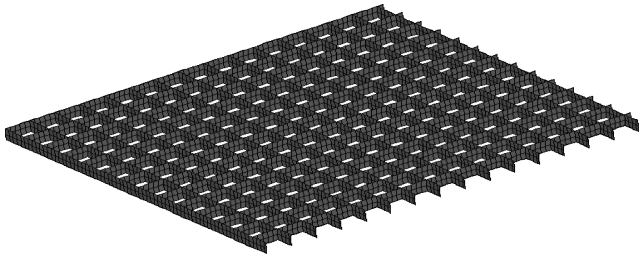

Fig. 6 Idealized flat double-skin cross-ribbed panel configuration.

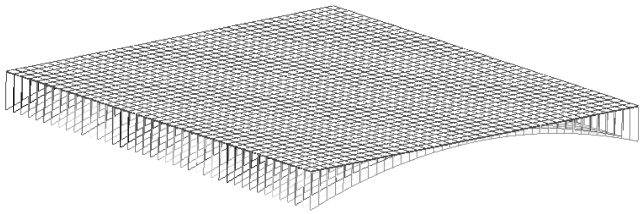

Fig. 7 Idealized flat honeycomb panel configuration with span-wise catenary.

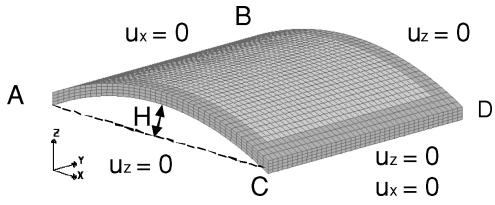

Fig. 8 Idealized spanwise vaulted shell with bar stiffener configuration showing second set of boundary conditions.

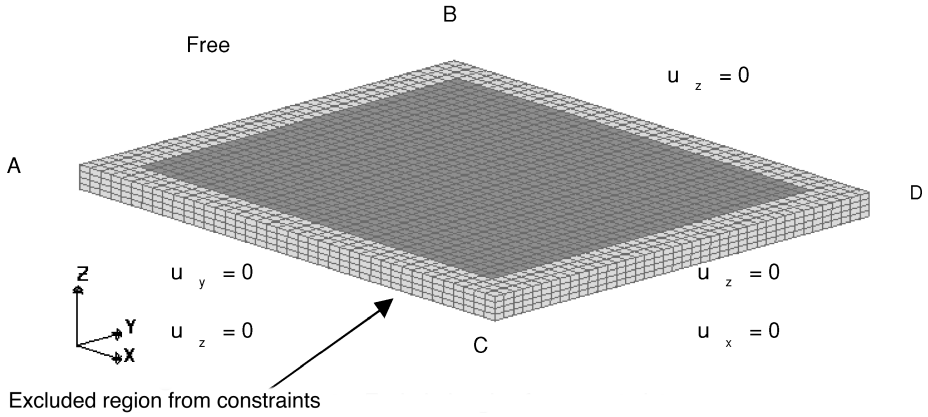

Fig. 5 Idealized flat honeycomb sandwich panel configuration showing first set of boundary conditions.

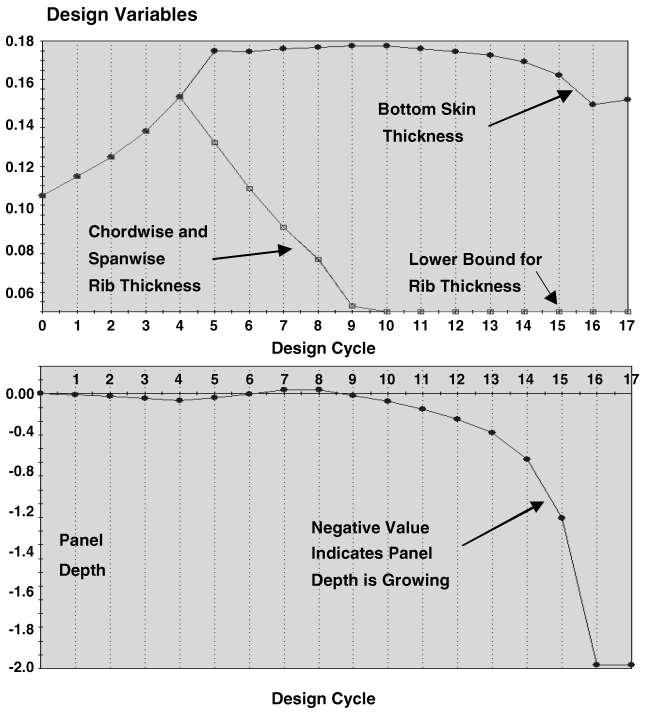

Fig. 9 Design variable history from initial results of a flat double-skin ribbed panel optimization with only stress constraints and pressure load.

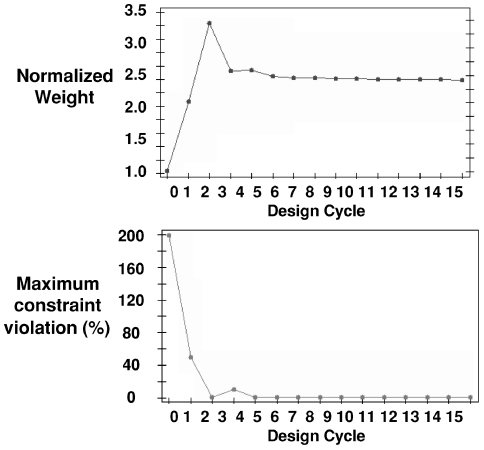

Fig. 10 Objective function and constraint violation history from initial results of a double-skin ribbed panel optimization under both stress and buckling constraints with combined compressive and pressure loads.

C. Flat Honeycomb Panel with Catenary Cable

A catenary cable support system with vertical rod connections to the honeycomb panel was used to reduce deflection, much like a suspension bridge, as shown in Fig. 7. However, optimization results were similar to the previous cases. Catenary cables were marginally beneficial for reducing lower skin thickness assuming that the deflections and loads keep the cable system in tension.

D. Spanwise Vaulted Shell with Rod Stiffener

This concept used a spanwise vaulted shell to contain pressure efficiently. Three spanwise bar elements were added for increasing buckling stiffness, as shown in Fig. 8. Spanwise vaulting also increases stiffness to compressive load; thus, it required less skin thickness but exhibited higher deflections.

The optimization results and weight estimates are shown in Table 1. These results were consistent with the two-dimensional nonlinear beam-column analyses from Eqs. (1–3) and with earlier design results presented in Ref. 5. Thus, it became apparent that inner cylindrical segments of fuselage were necessary in order to contain pressure efficiently through membrane stress. The membrane in-plane forces at the fuselage junction could be symmetrically balanced in tension using the intercabin wall, thus avoiding major bending stresses at the junction. Thus, the outer superstructure at the top and bottom part of the fuselage could be used to resist the spanwise bending load yet retain aerodynamic shape and smoothness. This led to the design of a set of multibubble structural concepts, as described next.

IV. Conventional Fuselage Analysis

Initially, a set of stiffened aluminum fuselage configurations shown in Figs. 6–9 was analyzed for acceptable stress and deflection using 127,530 Pa (18.6 psi) internal pressure loads only. These finite element models were developed in-house and analyzed using a tool described in Ref. 13. An idealized Airbus A380 elliptic-section fuselage and a baseline cylindrical-section fuselage with hoop stiffeners, shown in Figs. 11 and 12, were first analyzed for comparison purposes.

A. Elliptic Section Fuselage

A 10-m-long section with three floors, as shown in Fig. 11, was analyzed first to compare cylindrical- versus elliptic-section fuselage strength characteristics under internal pressure. The 8.5-m-high, 7-m-wide Airbus A380-type stiffened elliptic section, shown in Fig. 11, was stiffened with 21 ring stiffeners, each 0.1 m deep at 0.5-m intervals. Thickness of skin and ring stiffeners was assumed to be 0.003 m. These values are generally typical for commercial transport aircraft.[10,12] Maximum displacement from the FEM analysis was about 0.153 m at top and bottom of the fuselage. The resulting nodal von Mises stresses at the shell element top surface are shown in Fig. 11. Average von Mises stress on the skin was of the order $3.5E+8$ Pa, which is 2.1 times the ideal hoop stress $pr \cdot D/2t$. No buckling analysis was done. FEM weight of this section was 3828 kg with total floor area of 177 m^2.

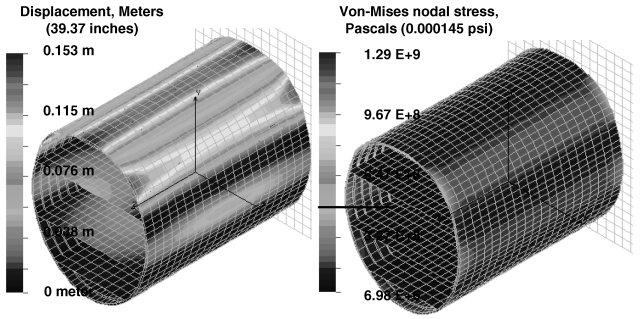

Fig. 11 A380-type 8.5 × 7 m^2 stiffened elliptic section fuselage: displacement and element nodal von Mises stresses due to 127,530 Pa (18.6 psi) internal pressure.

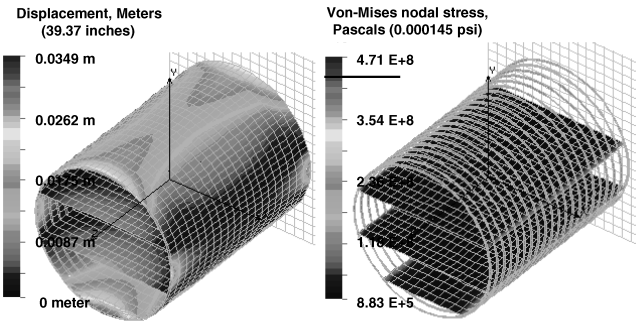

Fig. 12 Baseline stiffened cylindrical fuselage: 7.75 m diameter, displacement and nodal von Mises stress due to 127,530 Pa (18.6 psi) internal pressure.

B. Cylindrical Section Fuselage

The cylindrical section with 7.75-m diameter, shown in Fig. 12, had the same circumference as the elliptic section. It was also stiffened with ring stiffeners, each 0.1 m deep at 0.5-m intervals. Thickness of skin and ring stiffeners was assumed to be 0.003 m. This cylindrical-section fuselage was also subjected to 127,530 Pa internal pressure. Figure 12 shows that maximum displacements are of the order 0.035 m. The resulting nodal von Mises stresses at the shell element top surface are also shown in Fig. 12. Average von Mises stress on the skin was of the order $2.6E+8$ Pa, which is about 1.5 times the ideal hoop stress given by $pr \cdot D/2t$. FEM weight of this section was 3943 kg with total floor area of 192 m^2. For this cylindrical section, FEM stresses were significantly lower and had higher floor area, although net weight was slightly higher.

V. Multibubble Fuselage Design

Based on the lessons learned from these analyses, a multibubble stiffened pressure vessel concept was developed. Diameters of the cylindrical segments were almost same as the cylindrical segment previously described. In this design the two merging bubble sections meet with the intercabin vertical wall at an angle so surface in-plane membrane forces are in self-equilibrium.[10] Thus, in an ideal case, the resulting membrane stresses on the cylindrical-section skin are balanced by tension in the intercabin walls. This geometrical arrangement could reduce undue bending at these joints, thereby preserving the advantage of a cylindrical-section fuselage, under internal cabin pressure. This special geometry results in three-floor multiaisle fuselage, each 5.8 m wide. In this and subsequent FEM models, cylindrical skin segments were stiffened with 10-cm-deep ring stiffeners that were modeled by beam3d elements. These I-beam stiffeners, with 5-cm-wide flange, 10-cm-deep web, and 3-mm-thick flange and web, were used at 0.5-m chordwise intervals on all cylindrical surfaces, intercabin walls, and floors. These values are generally typical for commercial transport aircraft.[10,12]

A. Four-Bubble Fuselage

This force-balanced bubble concept was examined for double and triple bubble configurations and then extended to a four-bubble three-floor concept with additional outer stiffened double panels at the top and bottom of the fuselage. These outer panels initially consisted of two stiffened shells 25 cm apart and were supported by the cylindrical inner fuselage sections at the midpoint. These outer shells were not connected to the intercabin vertical walls directly, as shown in Fig. 13 at top. The outer shell was added to provide bending and buckling stiffness to spanwise bending loads that were not considered in the double- and triple-bubble concepts. This model was subjected to the standard 84,835-Pa internal cabin pressure and is denoted load case 1. For load case 2, top stiffened panels were subjected to 164,350 kg/m spanwise compressive loads. Equal and opposite tensile loads were applied at bottom panels to represent an equivalent maximum estimated bending moment.

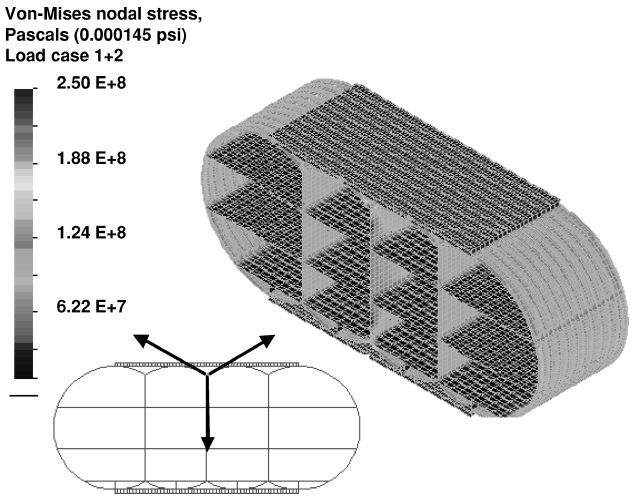

Fig. 13 Four-bubble fuselage concept: element nodal von Mises stress at top due to 84,835 Pa (12.3 psi) internal cabin pressure and 164,350 kg/m (9200 lbs/in) spanwise compressive load on top panel and equal tensile load at bottom panel.

Figure 13 shows element nodal von Mises stress at the top due to 84,835 Pa internal cabin pressure and 164,350 kg/m spanwise compressive load on the top panel and equal tensile load at the bottom panel. Maximum displacement was of the order 0.015 m and maximum stress was of the order $2.5E+8$ Pa. Skin thickness was assumed to be 0.003 m except for that of outer double wall, which was 0.005 m. Total weight of this section (8.25 m high, 19.325 m wide, 5 m long) was about 11,000 kg. The buckling safety factor was not satisfied for the assumed boundary condition. To increase buckling stiffness, cross ribs were later added (Fig. 13) to the outer double walls at 0.25-m chordwise intervals and 0.18-m spanwise intervals. FEM weight was 13,100 kg with cross ribs; the total floor area was 267 m^2. The buckling safety factor was about 1.0 for the compressive load. However, undesirable lower local bucking modes of the cargo floor panel for reversed loading were present. Overall, this design was better but not totally satisfactory.

B. Five-Bubble Double-Wall Fuselage

The five-bubble configuration shown in Fig. 14 was conceived and analyzed with internal design pressure loads as well as with estimated equivalent compressive loads on the top panels (and equal tensile load on the bottom panels) due to fuselage bending to obtain acceptable stress, deflection, and buckling stability safety factor. Based on plate buckling analysis[11,12] the top and bottom double-wall depth was chosen as 0.15 m with 0.003-m-thick spanwise running ribs at 0.25-m intervals. The radius of the inner cabin vaulted ceiling was reduced from 3.875 to 3.75 m. The radius of the outer cabin was calculated to be 3.248 m in order to get approximate membrane stress equilibrium at outboard joints. Additional spanwise running tie rods were also used at the top and bottom of the cabin. Because only half the fuselage was modeled, symmetric clamped boundary conditions were assumed at the plane of symmetry.

Initial results of the redesigned multibubble fuselage appear to be interesting. Maximum displacements were of the order of 0.014 m at the outer cabin walls and inside vaulted ceiling midspan. Figure 15 shows the von Mises stress distribution at element nodes computed

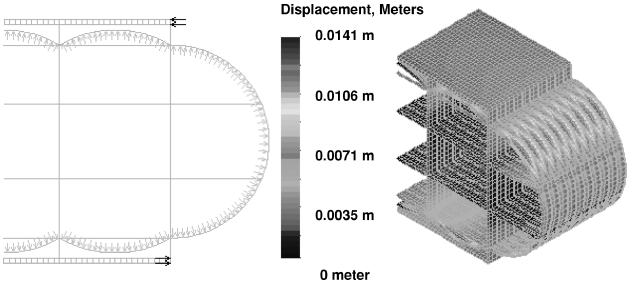

Fig. 14 Five-bubble fuselage with ribbed outer double wall: force-balanced stiffened fuselage concept.

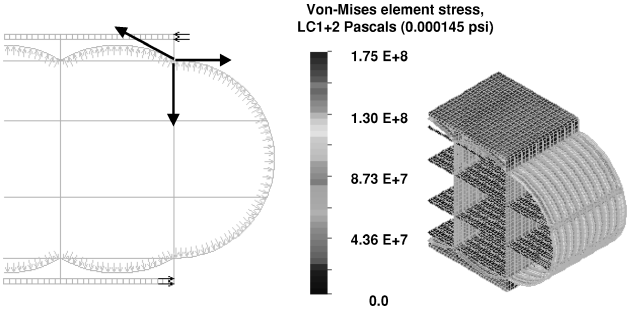

Fig. 15 Five-bubble fuselage with ribbed outer wall: element nodal von Mises stress distribution at top surface due to 84,835 Pa internal cabin pressure and 164,350 kg/m spanwise compressive load on top panel and equal tensile load at bottom panel.

on the top surface due to combined internal cabin pressure and spanwise compressive load on the top panel and equal tensile load at the bottom panel. The maximum stresses were of the order of $1.75E+8$ Pa. These stresses were well within allowable limits and about 25% lower than the four-bubble design with about 10% increase in unit weight/floor area. The buckling safety factor for pressure alone was -1.0, indicating cylindrical shell buckling for a reversed pressure direction. With this cross-ribbed outer wall design, which was similar to those of the panel shown in Fig. 6, buckling safety factors with the design compressive load were satisfactory. However, the fine-mesh FEM model exhibited many lower local plate buckling modes due to the manner in which the compressive forces were applied at nodes, in order to represent bending loads approximately. The vertical supports between outer double-wall and vertical cabin walls exhibited many lower local panel buckling modes with buckling safety factors starting from 0.7 to 1.95 for the first 20 modes. The total weight of this half FEM model was about 5176 kg with a floor area of 115 m^2.

VI. Unit Weight Comparison

It was difficult to make a fair comparison of different concepts that were analyzed due to the fact that each concept was a different model of a particular component of the fuselage with their own representative loading and boundary conditions and did not include wing structure or other super structures. However, an initial attempt was made to estimate the fuselage component unit FEM weight per unit payload floor area and observe the trend. A summary of this comparison is shown in Fig. 16.

These relative unit weights were computed as the ratio of the total finite element weight of the structure divided by floor areas inside the fuselage section. The first three concepts, labeled BWB Bay 3, show weights of the vaulted shell with heavy honeycomb, flat sandwich shell with heavy honeycomb core (FHHC), and vaulted ribbed shell, and also included side walls, and front and rear pressurized spar of similar construction.[5] It should be noted that these previous designs were not optimized or analyzed for buckling stability, although sizing was done using two-dimensional nonlinear beam-column analysis similar to that described earlier in the Paper.

For all the cylindrical, elliptic, and multibubble concepts, the total FEM weight was divided by floor area, which included two passenger floors and one cargo floor, in order to obtain the unit weight ratio. Unlike previous BWB Bay 3 analysis, weights did not include pressure bulkhead. For the case of the heavy honeycomb core rectangular panel described earlier in Fig. 5, FEM-based weight was multiplied by 2 to account for bottom panel, floor, side walls, or pressure-bearing spar for an approximate equitable comparison. This modified weight was simply divided by panel area to get the unit weight ratio shown in the figure. These estimates appear consistent with that of the FHHC case studied previously.[5] As a rule of thumb, FEM-based weights are generally 40–50% lower than an actual fabricated structure. However, this unit weight comparison confirms two previously known hypotheses and provide some quantitative values, namely, 1) the multibubble noncylindrical pressure vessel configurations appear to be twice as inefficient compared to cylindrical structure, and 2) proper integration of partially cylindrical surfaces in pressurized fuselage design could reduce the overall weight by about 20–30% compared to using all flat surfaces.

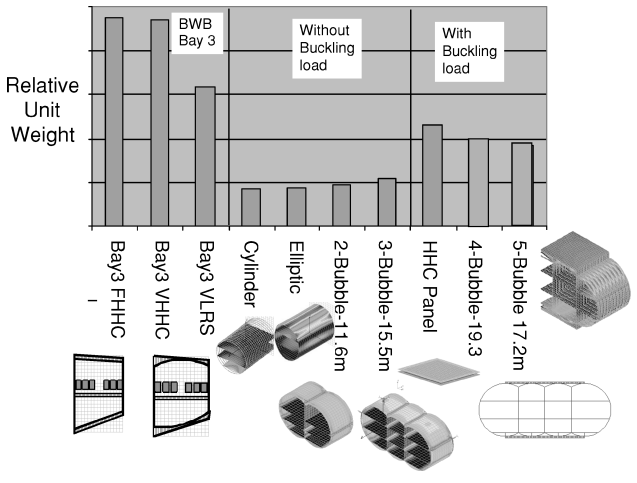

Fig. 16 Relative normalized unit weight comparison of finite element model (FHHC, flat sandwich shell with heavy honeycomb core; VHHC, vaulted shell with heavy honeycomb core; VLRS, vaulted ribbed shell; HHC, heavy honeycomb core).

VII. Conclusions

A set of structural concepts for pressurized fuselage of BWB-type flight vehicles was presented. A multibubble fuselage configuration concept was developed for balancing internal cabin pressure load efficiently through balanced membrane stress in inner cylindrical-segment shells and intercabin walls. To provide buckling stability and carry spanwise bending loads, additional cross-ribbed outer shell structures appear to be quite effective. Thus, it was advantageous to use the inner cylindrical shells for pressure containment and let the outer shells resist overall bending. This decoupling may enable both components to stay in a membrane state of stress with minimal bending. The duct space between the inner and outer shell could be used for a direct ventilation system with potential weight and power savings. However, in the case of a cabin pressure leak during flight, the outer ribbed shell was found to be strong enough to withstand operational cabin pressure, thus providing adequate redundancy. Venting the duct space through pressure valves in this regard could also provide an additional safeguard. Nevertheless, further studies for refinement and optimization of these concepts are necessary for gaining acceptance by the industry.

Acknowledgments

The authors thank Dennis Bushnell for funding this project through the Director's "Creativity and Innovation" Initiative Fund. Special thanks are also due to Robert Liebeck and Sean Wakayama of Boeing Company and Gary Vanderplaats of Vanderplaats R&D, Inc., for their insight and critique.

References

[1]Liebeck, R. H., "Blended-Wing-Body Technology Study," Final Rept. NASA Contract NAS1-20275, Boeing Rept. CRAD-9405-TR-3780, The Boeing Co., Long Beach, CA, Oct. 1997.

[2]Liebeck, R. H., Page, M. A., and Rawdon, B. K., "Blended-Wing-Body Subsonic Commercial Transport," AIAA Paper 98-0438, Jan. 1998.

[3]Dorsey, J. T., Wu, C. K., Rivers, K. H., Martin, C. J., Jr., and Smith, R., "Airframe Integration Trade Studies for a Reusable Launch Vehicle," Paper 247, Space Technology and Applications International Forum (STAIF 99), American Inst. of Physics, Melville, NY, 1999.

[4]Hitch, H. P. Y., "Pressure Cabins of Elliptic Cross Section," *Aeronautical Journal*, Vol. 92, No. 916, 1988, pp. 207–223.

[5]Mukhopadhyay, V., "Structural Concepts Study of Non-Circular Fuselage Configurations," *Proceedings of the 1st AIAA/SAE World Aviation Congress*, SAE Aerospace International, Warrendale, PA, Oct. 1996; also SAE Paper WAC-67, Oct. 1996.

[6]Wakayama, S., and Kroo, I., "The Challenge and Promise of Blended-Wing-Body Optimization," *Proceedings of the 7th AIAA Symposium on Multidisciplinary Analysis and Optimization*, AIAA, Reston, VA, Sept. 1998, pp. 239–250; also AIAA Paper 98-4736, Sept. 1998.

[7]Morrocco, J. D., and Flottau, J., "Europe Seeks Global Leadership in Aeronautics," *Aviation Week and Space Technology*, edited by M. N. David, Vol. 156, No. 5, 2001, pp. 30, 31.

[8]Timoshenko, S. P., and Gere, J. M., "Theory of Elastic Stability," McGraw–Hill, New York, 1961, Chap. 1, pp. 1–11.

[9]*GENESIS V6.0: Structural Analysis and Optimization*, *Overview* and *Reference*, Vols. 1 and 2, Vanderplaats R&D, Colorado Springs, CO, 2000.

[10]Bruhn, E. F., "Analysis and Design of Flight Vehicle Structures," Tri State Offset Co., Cincinnati, Ohio, 1965, Chap. A16, pp. A16.1–A16.9 and Chap. C11, pp. C11.29–C12.51.

[11]Young, Y. C., "Roark's Formulas for Stress and Strain," McGraw–Hill, New York, 6th ed., 1989, Chap. 12, pp. 515–643.

[12]Niu, M. C. Y., "Airframe Structural Design," Conmilit Press Ltd., Hong Kong, 1993, Chap. 11, pp. 376–428.

[13]*COSMOS/M Basic FEA System User's Guide*, Structural Research and Analysis Corporation, Santa Monica, CA, 1993.